Inertia-induced dendriticlike patterns in lifting Hele-Shaw flows

Pedro H. A. Anjos, Eduardo O. Dias,* and José A. Miranda†
Departamento de Física, Universidade Federal de Pernambuco, Recife, Pernambuco 50670-901, Brazil
(Received 15 July 2016; published 20 January 2017)

The lifting Hele-Shaw cell problem is a variant of the classical constant-gap Hele-Shaw situation in which the cell gap width is time dependent. Experiments on Newtonian fluid flows in lifting Hele-Shaw cells with large lifting velocities reveal the development of dendriticlike fingered structures that compete among themselves. The usual Darcy law description of the problem, where inertial effects are neglected, has not been able to explain the origin of these competing sidebranched patterns. In this work we use a generalized Darcy law and a perturbative mode-coupling theory to investigate the impact of inertia on the pattern-forming dynamics of the system. Two main results are deduced: Inertia induces a mechanism for finger sidebranching formation and favors the intensification of finger competition events.

DOI: 10.1103/PhysRevFluids.2.014003

I. INTRODUCTION

The displacement of a fluid by another is one of the most common processes involving the development of interfacial instabilities. One of the simplest and best studied instabilities occurring at the interface between two fluids is the Saffman-Taylor (or viscous fingering) problem [1,2]. It comprises a situation in which a more viscous fluid is displaced by a less viscous one, in the narrow space confined between two parallel plates of a Hele-Shaw cell. Under such circumstances, the two-fluid interface becomes unstable and the lower viscosity fluid penetrates the other in a pattern resembling a set of fingers. These fingers proliferate and develop further into complex patterns. The problem was originally studied by considering the longitudinal flow in a rectangular channel [1–8], where the system evolved until a single dominating stable finger was formed. Another very popular Hele-Shaw flow setup is the so-called radial (or circular) geometry [9–14], in which an axisymmetric fluid injection takes place, leading to the formation of multiply branched structures, markedly characterized by the spreading and splitting of the growing fingers.

In addition to the traditional rectangular and radial Hele-Shaw flow configurations, a third geometry has also attracted considerable attention: the lifting Hele-Shaw cell arrangement [15–27]. In contrast to the conventional versions of the problem, which consider flow in constant-gap Hele-Shaw cells, the lifting situation addresses fluid displacement in variable-gap cells. In the lifting case, initially one has a circular interface separating a more viscous fluid surrounded by a less viscous one. Then, while the lower cell plate is held fixed, the upper plate is lifted parallel to it, establishing a time-dependent gap flow. During the lifting process, the outer fluid enters the gap through the sides and displaces the inner fluid, making the interface unstable via the Saffman-Taylor instability. As a consequence, the contracting interface deforms as the fingers of the outer fluid invade the inner fluid. Eventually, the amplitude of the perturbations increases and longer fingers of the outer fluid move towards the center of the cell. As time advances, eye-catching fingering patterns are formed.

For lifting Hele-Shaw flow with Newtonian fluids, one normally observes penetrating fingers presenting smooth boundaries and slightly inflated tips. These invading fingers clearly compete

*eduardodias@df.ufpe.br
†jme@df.ufpe.br

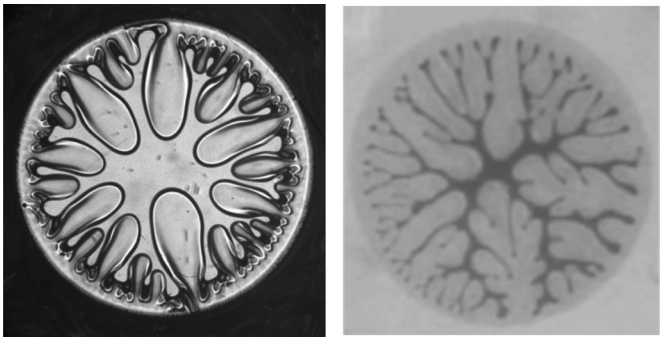

FIG. 1. Illustrative examples of advanced time experimental patterns for lifting Hele-Shaw flow with Newtonian fluids. The left panel shows smooth shaped penetrating fingers obtained for low lifting velocities (reprinted from Fig. 6 of Ref. [25] with the permission of AIP Publishing). The right panel shows convoluted, dendriticlike invading fingers (clear fluid) formed at high lifting speeds [reprinted from Fig. 2(b) in Ref. [23] with the permission of Springer].

among themselves, reaching different lengths [19,22,25]. For a typical illustration of these patterns, see the left panel of Fig. 1. Such nonsplitting fingering patterns are considerably distinct from the markedly branched structures usually obtained for injection-induced radial flows in fixed-gap Hele-Shaw cells [9–14]. These distinguishing morphological features of the Newtonian lifting flow system have been largely documented in the literature through laboratory experiments and intensive numerical simulations (see [15–27], and references therein).

Despite the recent effort devoted to improving the understanding of Saffman-Taylor instabilities in Newtonian lifting Hele-Shaw flows [15–27], some important experimental findings still lack a theoretical explanation. One emblematic example is the following: Newtonian fluid experiments such as the ones performed in Refs. [20,23,28] for large lifting velocities have revealed pattern-forming structures that are completely different from the ones normally obtained in Refs. [15–27], where lower lifting speeds have been utilized. For large lifting speeds, instead of generating nonsplitting, smooth penetrating fingers, one encounters much more convoluted, dendriticlike fingering structures notably characterized by the occurrence of sidebranching (i.e., fingers presenting lobes branching out sideward). For an illustrative prototype of sidebranching pattern formation in Newtonian lifting Hele-Shaw flows, see the right panel of Fig. 1. Even though it is well known that such fractal-like dendritic fingering shapes can be produced during injection-driven radial flows in constant-gap Hele-Shaw cells [29–36], as well as for displacements in lifting Hele-Shaw cells [37–39] for *non-Newtonian* fluids, they do not arise when the fluids are Newtonian and the lifting velocities are low. A theoretical explanation for the growth of competing sidebranching, dendriticlike fingers in lifting Hele-Shaw flow for Newtonian fluids is still lacking.

In this work, our main purpose is to offer a theoretical description that could justify the appearance of such dendriticlike patterns in confined lifting flows with Newtonian fluids. During the course of this paper, we will deduce that the development of sidebranching at the fluid-fluid interface is induced by inertial effects. The vast majority of studies in Hele-Shaw cells neglect the influence of inertia. This is justified by the fact that, under customary Hele-Shaw conditions (i.e., low flow velocities, small gap width, highly viscous displaced fluid, etc.), one has a nearly zero Reynolds number situation, so the action of inertia can be safely neglected. In this noninertial framing, the fluid motion is perfectly described by Darcy's law, which connects, in a very simple fashion, the fluid velocity to the pressure gradient. However, this is not always the case. If the conditions are such that the flow velocity is considerably high, the cell gap thickness is not so small, or if the displaced fluid is not excessively viscous, one can have a sizable Reynolds number flow where inertial effects cannot be discarded. Of course, under a non-negligible Reynolds

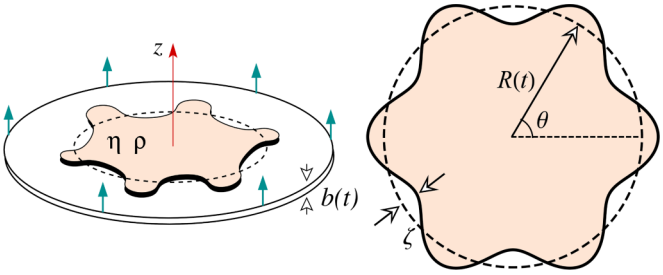

FIG. 2. Schematic representation of the lifting (time-dependent gap) Hele-Shaw flow setup (left) and upper view of the lifted inner fluid droplet (right).

number scenario, the usual Darcy law description of the viscous fingering problem is no longer valid.

Recently, there has been growing interest in the impact of inertial effects on the development of the Saffman-Taylor instability [40–48]. By using experiments and analytical and numerical methods, these studies analyzed various Hele-Shaw flow situations where inertia plays a relevant role. In these cases, a more elaborate, modified Darcy description has been derived based on the gap averaging of the three-dimensional (3D) Navier-Stokes equation for the system. The consideration of inertia resulted in the emergence of suggestive dynamical responses regarding the linear stability and the morphology of the interfacial patterned structures: While at the linear level inertia tends to stabilize interface disturbances, at nonlinear stages inertial effects can widen the fingers [43,44,46]. It should be noted that these studies of the role of inertia have focused on *constant-gap* Hele-Shaw cells, for injection-driven rectangular and radial flows and radial flows in the rotating Hele-Shaw setup. However, the analysis of the effects of inertia in *variable-gap* Hele-Shaw flows and the understanding of how they affect key features of the pattern-forming dynamics still need to be examined. That is exactly what we aim to do in this work.

The remainder of this paper is structured as follows. Section II presents the derivation of the weakly nonlinear equations for lifting Hele-Shaw flows with Newtonian fluids, when inertial effects are taken into account. This is done by employing a second-order perturbative mode-coupling approach, which allows one to access the onset of intrinsically nonlinear pattern-forming mechanisms. The linear stability aspects of the system are briefly examined in Sec. III. Then, in Sec. IV, relevant information about the influence of inertia on the development of nonlinear sidebranching structures, as well as on the finger competition dynamics, is introduced and discussed. Finally, Sec. V summarizes our main results and provides some concluding remarks.

II. MODE-COUPLING DIFFERENTIAL EQUATION

The basic geometry of the lifting cell problem is sketched in Fig. 2. Consider a variable-gap Hele-Shaw cell containing a Newtonian, viscous, incompressible fluid of viscosity η and density ρ, surrounded by another fluid of negligible density and viscosity. Between the two fluids there exists a surface tension σ. At time $t = 0$ the fluid-fluid interface is circular and has initial radius $R(t = 0) = R_0$, while the initial plate spacing is represented by $b(t = 0) = b_0$. Then, at time $t > 0$ the upper cell plate is lifted along the direction perpendicular to the plates (z axis) and the lower plate is held fixed. The plate separation procedure is carried out in such a manner that the plates always remain parallel to each other.

As the upper plate is moved upward, the outer fluid is sucked in and the circular interface retracts, becoming unstable due to the Saffman-Taylor instability. The perturbed fluid-fluid interface is described as $\mathcal{R}(\theta,t) = R(t) + \zeta(\theta,t)$, where θ represents the azimuthal angle and $R(t)$ is the time-dependent unperturbed radius. Volume conservation provides a useful relation between $R(t)$ and the time-dependent cell gap width $b(t)$: $R^2(t)b(t) = R_0^2 b_0$. In addition, $\zeta(\theta,t) = \sum_{n=-\infty}^{+\infty} \zeta_n(t) \exp(in\theta)$

denotes the net interface perturbation with Fourier amplitudes $\zeta_n(t)$ and integer wave numbers n. Note that, in contrast to purely linear stability analyses (which are linear, i.e., first order, in ζ), our weakly nonlinear approach keeps terms up to the second order in ζ. This allows one to explore the development of key morphological aspects of the emerging interfacial patterns at the early nonlinear stages of the dynamics [8,12].

To examine the impact of inertia on the Newtonian lifting Hele-Shaw cell problem, we follow the theoretical approach developed in Refs. [40–48] and consider that the fluid flow is governed by a nonlinear generalized Darcy law equation

$$\rho\left[\frac{\partial \mathbf{u}}{\partial t}+\frac{6}{5}(\mathbf{u}\cdot\boldsymbol{\nabla})\mathbf{u}\right]=-\boldsymbol{\nabla} p-\frac{12\eta}{b^2}\mathbf{u}, \tag{1}$$

where $\mathbf{u}$ denotes the 2D fluid velocity and p is the 2D pressure. This generalized version of Darcy's law has been derived by averaging the 3D Navier-Stokes equation over the gap direction and retaining its inertial terms. The coefficients appearing in front of the terms $\partial\mathbf{u}/\partial t$ and $(\mathbf{u}\cdot\boldsymbol{\nabla})\mathbf{u}$ in Eq. (1) may vary, depending on the way the gap averaging is performed, but are always of order 1 [40–48].

Additionally, we consider a modified 2D continuity equation for an incompressible fluid [15,17]

$$\boldsymbol{\nabla}\cdot\mathbf{u}=-\frac{\dot{b}(t)}{b(t)}, \tag{2}$$

where $\dot{b}(t)=db(t)/dt$ is the upper plate velocity along the z axis. Notice that, by taking the time derivative of the volume conservation expression $R^2(t)b(t)=R_0^2 b_0$, one obtains a helpful connection between the velocity of the contracting unperturbed interface $\dot{R}(t)=\dot{R}$ and the velocity of the upper plate $\dot{b}$ through the relation $\dot{R}=-(\dot{b}R)/2b$.

By taking into consideration the potential nature of the flow [43,44], Eq. (1) can be conveniently rewritten as

$$\rho\left[\frac{\partial\phi}{\partial t}-\frac{3}{5}|\boldsymbol{\nabla}\phi|^2\right]=p-\frac{12\eta}{b^2}\phi, \tag{3}$$

where ϕ is a velocity potential. By substituting $\mathbf{u}=-\boldsymbol{\nabla}\phi$ into Eq. (2), one can verify that ϕ obeys the Poisson equation $\nabla^2\phi=\dot{b}/b$, having the solution

$$\phi(r,\theta)=\sum_{n\neq 0}\phi_n(t)\left(\frac{r}{R}\right)^{|n|}e^{in\theta}+\frac{\dot{b}r^2}{4b}. \tag{4}$$

Two boundary interfacial conditions complete the definition of the moving boundary problem, namely, the Young-Laplace boundary condition [2], which expresses the pressure jump across the fluid-fluid interface $r=\mathcal{R}$,

$$p=\sigma\kappa, \tag{5}$$

where the in-plane interfacial curvature is denoted by κ, and the kinematic boundary condition

$$\frac{\partial\mathcal{R}}{\partial t}=\left[\frac{1}{r^2}\frac{\partial r}{\partial\theta}\frac{\partial\phi}{\partial\theta}-\frac{\partial\phi}{\partial r}\right]_{r=\mathcal{R}}, \tag{6}$$

which states that the normal components of each fluid's velocity are continuous at the interface [2,9].

Now we have all necessary elements to find a mode-coupling differential equation that describes the time evolution of the interfacial amplitudes $\zeta_n(t)$. First, we express ϕ [Eq. (4)] in terms of the perturbation amplitudes ζ_n by considering the kinematic condition (6). Substituting the resulting relations and the pressure jump condition (5) into Eq. (3), always keeping terms up to second order in ζ, and Fourier transforming, we obtain the *dimensionless* equation of motion for the perturbation

amplitudes (for $n \neq 0$)

$$\mathrm{Re}\ddot{\zeta}_n + \left[\frac{1}{b^2} - \mathrm{Re}\frac{\dot{b}}{10b}|n|\right]\dot{\zeta}_n - \left\{\Lambda(n) + \mathrm{Re}\frac{1}{2b}(|n|-1)\left[\ddot{b} - \frac{3\dot{b}^2}{2b}\right]\right\}\zeta_n$$
$$= \sum_{n'\neq 0}[F(n,n') + \mathrm{Re}H(n,n')]\zeta_{n'}\zeta_{n-n'} + \sum_{n'\neq 0}\left[\frac{1}{b^2}G(n,n') + \mathrm{Re}I(n,n')\right]\dot{\zeta}_{n'}\zeta_{n-n'}$$
$$+ \mathrm{Re}\sum_{n'\neq 0}[G(n,n')\ddot{\zeta}_{n'}\zeta_{n-n'} + J(n,n')\dot{\zeta}_{n'}\dot{\zeta}_{n-n'}], \tag{7}$$

where $\Lambda(n) = (|n|-1)(\dot{b}/2b^3) - b^{3/2}|n|(n^2-1)/q^3\mathrm{Ca}$,

$$\mathrm{Re} = \frac{\rho b_0 \dot{b}_0}{12\eta} \tag{8}$$

defines a Reynolds number that quantifies the effect of inertia on the system, $\dot{b}_0 = \dot{b}(0)$,

$$\mathrm{Ca} = \frac{12\eta\dot{b}_0}{\sigma} \tag{9}$$

is a capillary number that measures the ratio of viscous and surface tension forces, and

$$q = \frac{R_0}{b_0} \tag{10}$$

represents the initial aspect ratio.

Furthermore, the mode-coupling terms are given by

$$F(n,n') = |n|b^{1/2}\left\{\frac{\dot{b}}{2b^3}\left[\mathrm{sgn}(nn') - \frac{1}{|n|} - \frac{1}{2}\right] - \frac{b^{3/2}}{q^3\mathrm{Ca}}\left[1 - \frac{n'}{2}(3n'+n)\right]\right\}, \tag{11}$$

$$G(n,n') = b^{1/2}\{|n|[\mathrm{sgn}(nn') - 1] - 1\}, \tag{12}$$

$$H(n,n') = |n|b^{1/2}\left(\frac{\dot{b}}{2b}\right)^2\left\{\frac{3}{5}\mathrm{sgn}[n'(n-n')] - \mathrm{sgn}(nn')\left[2\left(1 - \frac{b\ddot{b}}{\dot{b}^2}\right) + \frac{|n|}{5}\right]\right.$$
$$\left. + \left(1 + \frac{2}{|n|}\right)\left(1 - \frac{b\ddot{b}}{\dot{b}^2}\right) + \frac{|n'|}{5}\right\}, \tag{13}$$

$$I(n,n') = |n|b^{1/2}\left(\frac{\dot{b}}{2b}\right)\left\{\frac{6}{5}\mathrm{sgn}[n'(n-n')] + \mathrm{sgn}[n(n-n')] + \left(1 - \frac{|n|}{5}\right)\mathrm{sgn}(nn')\right.$$
$$\left. + \frac{|n'|}{5} - \frac{2}{|n|} - 1\right\}, \tag{14}$$

and

$$J(n,n') = b^{1/2}\left\{\tfrac{3}{5}|n|[\mathrm{sgn}[n'(n-n')] - 1] + |n|\mathrm{sgn}(nn') - 1\right\}, \tag{15}$$

where the sgn function equals ± 1 according to the sign of its argument. We have nondimensionalized Eqs. (7)–(15) as follows: (i) In-plane lengths are rescaled by R_0, (ii) $b(t)$ is scaled on its initial value b_0, and (iii) likewise, time is rescaled by the characteristic time $T = b_0/|\dot{b}_0|$. We direct the reader's attention to the fact that, for the rest of this paper, we use the dimensionless version of all the equations.

Equations (7)–(15) constitute one of the central results of this work, offering the time evolution of the perturbation amplitudes $\zeta_n(t)$ accurate to second order, incorporating the action of inertial effects into the Newtonian lifting Hele-Shaw cell problem. To one's advantage the system is neatly

described by three governing physical parameters Re, Ca, and q. Notice that when $\mathrm{Re} = 0$, Eq. (7) reproduces the simpler results obtained in Ref. [24] for the corresponding problem without inertia. It is worth noting that, if $\mathrm{Re} = 0$, $b^2\Lambda(n)$ represents the linear growth rate of the noninertial system. Throughout our study, as in most experimental and theoretical studies in lifting Hele-Shaw flows [18,19,21,22,25], we assume a constant lifting speed, so $b = 1 + t$.

We point out that, with respect to Hele-Shaw systems, the original idea related to the truncation of the infinite coupling to just second order is not actually ours, but has been proposed some time ago by other authors, for the rectangular Hele-Shaw geometry [49,50]. This fact has been also acknowledged in Ref. [8]. Then Miranda and Widom [12] extended the second-order weakly nonlinear analysis to the radial Hele-Shaw (injection-induced) geometry. More recently, Alvarez-Lacalle *et al.* [51,52] used a slightly different second-order weakly nonlinear scheme to investigate pattern formation in various Hele-Shaw cell configurations. It should be noted that the use of second-order weakly nonlinear analyses is also popular in the study of pattern formation in solidification [53,54]. We refer the readers to Refs. [8,12,49–54] to find useful detailed information about the perturbative series' criteria of smallness of parameters, convergence properties, and other technical aspects of the weakly nonlinear theory.

III. INFLUENCE OF INERTIA AT THE LINEAR REGIME

Although our current study focuses on the intrinsically nonlinear aspects of the interface dynamics, directly connected to the morphology of the emerging patterns, in this section we briefly discuss the purely linear part (i.e., linear in ζ) of the equation of motion (7),

$$\mathrm{Re}\ddot{\zeta}_n + \left[\frac{1}{b^2} - \mathrm{Re}\frac{\dot{b}}{10b}|n|\right]\dot{\zeta}_n - \left\{\Lambda(n) + \mathrm{Re}\frac{1}{2b}(|n|-1)\left[\ddot{b} - \frac{3\dot{b}^2}{2b}\right]\right\}\zeta_n = 0. \tag{16}$$

Equation (16) is a second-order ordinary differential equation (ODE), presenting time-dependent coefficients (in view that b is time dependent). This is in contrast to the considerably simpler equivalent first-order ODE obtained in the usual vanishing Reynolds number limit of the lifting Hele-Shaw cell problem [15–27]. Consequently, contrary to the noninertial lifting case ($\mathrm{Re} = 0$), already at the linear level, it is not easy to obtain closed form analytical expressions for the linear growth and stability of the system when $\mathrm{Re} \neq 0$.

However, useful information about the influence of inertia at the linear regime can be extracted from the linear growth rate $\lambda(n) = [\dot{\zeta}_n/\zeta_n]$, which can be numerically evaluated by utilizing Eq. (16). Figure 3 plots the linear growth rate $\lambda(n)$ as a function of the Fourier mode n, for three increasingly larger values of the Reynolds number. This is done by considering characteristic physical parameters $\mathrm{Ca} = 2.5 \times 10^{-4}$ and $q = 10^3$, taken at time $t = 1.3$. By examining Fig. 3, one can verify that the wave number of the fastest growing mode $n_{\max}$ [i.e., the mode n associated with the maximum value of $\lambda(n)$] is just slightly increased ($31 \leqslant n_{\max} \leqslant 35$) when Re is varied from 0 to 0.1. Since $n_{\max}$ is connected to the typical number of interfacial fingers rising at the linear level [22,25,26], one anticipates that the number of emerging fingers should not be significantly influenced by the action of inertia. On the other hand, the magnitude of the growth rate of maximum growth $\lambda(n_{\max})$ is considerably reduced when Re is increased, indicating that inertia would tend to stabilize the system.

Moreover, by observing Fig. 3 one can see that the critical mode n_{crit} of the system, i.e., the mode for which $\lambda(n) = 0$, is also only modestly increased ($54 \leqslant n_{\mathrm{crit}} \leqslant 60$) when Re changes from 0 to 0.1. Therefore, the width of the band of unstable modes (region of Fourier modes within the interval $0 \leqslant n \leqslant n_{\mathrm{crit}}$) just widens a little when Re assumes larger values. So, as in the case of $n_{\max}$, n_{crit} is not dramatically altered when Re is varied. In contrast, as mentioned above, the magnitude of the maximum growth rate $\lambda(n_{\max})$ is substantially diminished by the action of inertia. Therefore, one can say that the major effect of inertia at the linear level is in fact to restrain the growth of interfacial disturbances.

These linear predictions for the current variable-gap Hele-Shaw situation are in line with similar results obtained for the constant-gap, injection-driven flow studied in Refs. [44,46], when inertial

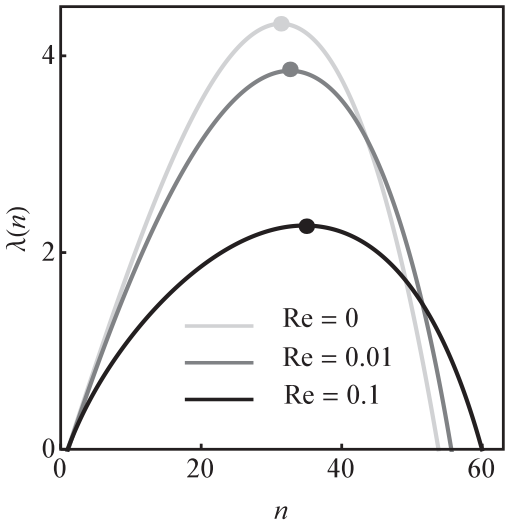

FIG. 3. Linear growth rate $\lambda(n)$ as a function of mode n, for three values of the Reynolds number Re. The maxima of the curves are indicated by circles. Here $\mathrm{Ca} = 2.5 \times 10^{-4}$, $q = 10^3$, and $t = 1.3$.

effects have been taken into account. Moreover, we have also found that the variable-gap system becomes increasingly unstable for higher values of Ca and q. Considering the mentioned difficulties in extracting analytical information about the lifting Hele-Shaw problem with inertia, the basic trends involving $n_{\max}$, n_{crit}, and $\lambda(n_{\max})$ are essentially what one can get at the purely linear level.

As one could imagine, the theoretical impediments regarding access to analytical results are even more serious in the description of the second-order weakly nonlinear dynamics, where the resulting mode-coupling expressions for the interacting modes [obtained from Eqs. (7)–(15)] are usually too lengthy and messy to be managed analytically. Despite this fact, our mode-coupling approach still allows one to gain insight into important morphological aspects of the emerging patterns under Newtonian lifting Hele-Shaw flows. This last point will become clear in the next section.

IV. EFFECT OF INERTIA ON NONLINEAR PATTERN-FORMING MECHANISMS

In this section we make use of Eqs. (7)–(15) and apply our weakly nonlinear theory to investigate how inertia may impact the shape of the emerging fingering patterns and the finger competition dynamics in the Newtonian lifting Hele-Shaw flow problem. To begin our discussion, it is convenient to rewrite the net interfacial perturbation in terms of cosine and sine modes

$$\zeta(\theta,t) = \zeta_0 + \sum_{n=1}^{\infty}[a_n(t)\cos(n\theta) + b_n(t)\sin(n\theta)], \tag{17}$$

where $a_n = \zeta_n + \zeta_{-n}$ and $b_n = i(\zeta_n - \zeta_{-n})$ are real valued. In the Fourier expansion (17), we include the $n = 0$ mode to maintain the area of the perturbed shape independent of the perturbation ζ. Within the scope of our second-order description, mass conservation imposes that the zeroth mode is written in terms of the other modes as [12]

$$\zeta_0 = -\frac{1}{4R}\sum_{n=1}^{\infty}\left[a_n^2(t) + b_n^2(t)\right]. \tag{18}$$

Without loss of generality we may choose the phase of the fundamental mode so that $a_n > 0$ and $b_n = 0$.

The most representative pattern-forming mechanisms of the viscous fingering instability, as they occur in noninertial, injection-driven Hele-Shaw flows, can be identified as spreading, splitting, and competition [2]. Some time ago it was shown that these basic nonlinear morphological mechanisms could be consistently reproduced by considering the weakly nonlinear coupling of just a few participating Fourier modes [8,12]: (i) The characteristic shape of the fingers (e.g., finger widening and narrowing) could be provided by the interplay between a fundamental mode n and its first-harmonic cosine mode $2n$, while (ii) finger competition events (related to finger length variability) could be described by the interaction of a fundamental mode n and its sine and cosine subharmonic modes $n/2$. Moreover, it has also been demonstrated that the mechanism of sidebranching formation for the flow of *non-Newtonian* (shear-thinning) [29–36] fluids in the injection-induced, radial Hele-Shaw problem (still neglecting inertial effects) would require the presence of mode $3n$ [34,36]. In this way, the dendriticlike growth detected in such non-Newtonian flows could be reproduced by considering the nonlinear coupling between a fundamental mode n and its harmonics $2n$ and $3n$. We direct the interested readers to Refs. [8,12,34,36] for a detailed discussion about the mode-coupling strategy, its description, and proposed interpretation of the typical pattern forming-mechanisms occurring in Hele-Shaw flows.

Before proceeding, we would like to make an important point about the weakly nonlinear results that will be presented in the rest of this work. One should not expect that our simulated weakly nonlinear interfacial patterns will quantitatively reproduce the fully nonlinear morphological features revealed in experimental realizations of the lifting Hele-Shaw problem, like the ones depicted in Fig. 1. These laboratory experiments focus on the fully nonlinear stages of pattern evolution, where the finger sizes are very large and the finger shapes are considerably complex. On the other hand, our perturbative weakly nonlinear analysis holds at the onset of nonlinearities, where the interfacial disturbances ζ must be significantly smaller than the corresponding unperturbed interfacial radius $R(t)$. In addition, in order to better understand and describe the mechanisms involved in the pattern formation process, our simulated weakly nonlinear interfaces consider the coupling of a small number of relevant Fourier modes. So we do not intend to precisely recreate the advanced time, extremely intricate lifting Hele-Shaw cell patterns detected experimentally. Of course, a perturbative Fourier analysis like ours would not be able to accomplish such a nontrivial task.

The main objective of our weakly nonlinear approach is to extract useful information about the complicated, fully nonlinear pattern-forming dynamics of the system, already at the lowest nonlinear order (i.e., at second order in ζ) and do that by describing the major pattern formation mechanisms (e.g., finger sidebranching and finger competition) by conveniently utilizing the interaction of just a few pertinent Fourier modes. Therefore, despite its limitations, the weakly nonlinear analysis presented here and in Refs. [8,12,34,36] is still useful in the sense that it can predict and capture the chief nonlinear behaviors that will eventually emerge at advanced time stages of the Hele-Shaw cell dynamics. It should be emphasized that the effectiveness of this particular weakly nonlinear strategy has been amply substantiated by a number of analytical, numerical, and experimental studies in the Hele-Shaw flow literature (see, for instance, Refs. [22,52,55–63]).

A. Inertia-induced sidebranching patterns

Our purpose here is to try to get valuable information about the possibility of producing dendriticlike sidebranching patterns in Newtonian lifting Hele-Shaw flows via the influence of inertia. As commented earlier, finger tip-narrowing, tip-broadening, and tip-splitting phenomena can be described by considering the influence of a fundamental mode n on the growth of its harmonic $2n$. It can be shown [24] that an enhanced tendency of the inward moving fingers of the outer fluid to get wider (narrower) occurs when $a_{2n} > 0$ ($a_{2n} < 0$). So a positive growth for the cosine amplitude of the first harmonic mode $2n$ would mean a tendency toward finger tip widening of the invading fingers of the outer fluid. Moreover, as proposed in Refs. [34,36], if the harmonic cosine mode amplitude a_{3n} is positive and sufficiently large, it can produce interfacial lobes branching out sideward, leading to sidebranching formation.

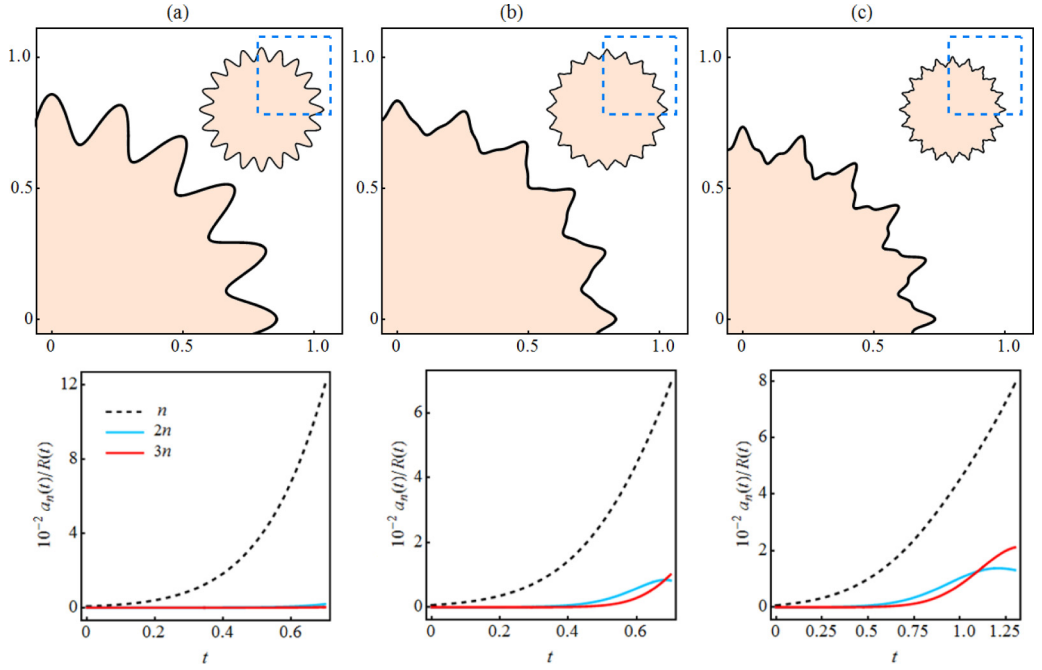

FIG. 4. Snapshot of the weakly nonlinear fluid-fluid interface (top panels), illustrating the typical fingering patterns that may arise during Newtonian lifting Hele-Shaw flows. A close-up view of the resulting patterns (for the areas delimited by dashed lines) is shown in the bottom left corner of each plot. The corresponding time evolution of the rescaled cosine amplitudes $a_n(t)/R(t)$ for modes n, $2n$, and $3n$, where $n = 20$, is depicted in the bottom panels. The values taken for the Reynolds number are (a) Re $= 0$, (b) Re $= 0.01$, and (c) Re $= 0.1$. In addition, Ca $= 2.5 \times 10^{-4}$ and $q = 10^3$. The final times used are (a) $t_f = 0.7$, (b) $t_f = 0.7$, and (c) $t_f = 1.3$.

So, to probe the possible resulting shapes of the fingers during Newtonian lifting Hele-Shaw flows with inertia, we consider the nonlinear coupling of the three morphologically relevant modes n, $2n$, and $3n$ and rewrite Eq. (7) in terms of the cosine amplitudes. As expected, the resulting mode-coupling equations are unfortunately pretty long and complicated. However, the time evolution of the amplitudes $a_n(t)$, $a_{2n}(t)$, and $a_{3n}(t)$ can be obtained by numerically solving such coupled nonlinear differential equations. Once this is done, the shape of the interface can be acquired by using Eqs. (17) and (18).

In Fig. 4 we illustrate the typical weakly nonlinear pattern morphologies that may emerge in lifting Hele-Shaw flows with Newtonian fluids if the effects of inertia are taken into consideration. In the top panels, we plot the shape of the contracting fluid-fluid interface for three increasing values of the Reynolds number Re. In order to facilitate the visualization of the morphological details of the resulting fingering structures, we plot the entire interface (for $0 \leqslant \theta \leqslant 2\pi$) in the top right corner of the panels plus a close-up view of part of it (for the angular sector $0 \leqslant \theta \leqslant \pi/2$) in the bottom left corner. Finally, in the bottom panels of Fig. 4, for each value of Re, we depict the time evolution of the rescaled cosine amplitudes $a_n(t)/R(t)$ for the three participating modes.

In Fig. 4 we take the initial conditions $a_n(0) = 6.5 \times 10^{-4}$ and $a_{2n}(0) = a_{3n}(0) = 0$ so that modes $2n$ and $3n$ are both initially absent. Likewise, we take $\dot{a}_n(0) = 6.2 \times 10^{-3}$ and $\dot{a}_{2n}(0) = \dot{a}_{3n}(0) = 0$. It worth pointing out that the values for the initial perturbation amplitudes are selected in such a way that the amplitudes for the first harmonic a_{2n} (responsible for setting the finger shape as wide or narrow) and harmonic a_{3n} (responsible for setting the sidebranching behavior) are considerably smaller (in this case they have been set to zero) than the amplitude of the fundamental mode a_n. Note that the fundamental mode mostly sets the initial n-fold symmetry for the pattern. This is

done to avoid artificial growth of modes a_{2n} and a_{3n} imposed solely by the initial conditions. In this way we guarantee that the interfacial behaviors we observe are spontaneously induced by the weakly nonlinear dynamics and not by artificially imposing large initial amplitudes for a_{2n} and a_{3n}. In addition, we take $\mathrm{Ca} = 2.5 \times 10^{-4}$, $q = 10^3$, and $n = 20$.

The patterns shown in Fig. 4 have been obtained after time has evolved in the interval $0 \leqslant t \leqslant t_f$, where t_f is the time at which successive interfaces are about to cross one another. Since this crossing is not detected in experiments and fully nonlinear simulations in lifting Hele-Shaw flows [22,25], we adopt the largest time before crossing as the upper bound time ($t = t_f$) for the validity of our theoretical description. The value of n ($n = 20$) used in Fig. 4 is obtained by setting $\lambda(3n) = 0$ for the highest Re and t_f (i.e., $\mathrm{Re} = 0.1$ and $t_f = 1.3$). This ensures that $3n$ is a critical mode at the largest time taken, so modes n, $2n$, and $3n$ will always remain inside the band of unstable modes during the entire lifting process.

Specifically, Fig. 4 considers the possible shapes assumed by the fingers for the following values of the Reynolds number: (a) $\mathrm{Re} = 0$, (b) $\mathrm{Re} = 0.01$, and (c) $\mathrm{Re} = 0.1$. First, we analyze the case in which inertial effects are completely neglected [Fig. 4(a)]. In this noninertial lifting scenario, nothing really exciting happens and reasonably unstructured fingers are formed. In the absence of inertia, the morphology of the inward moving fingers is basically determined by the growth of the fundamental mode n, which reaches much larger amplitudes than the modes $2n$ and $3n$. This is clearly illustrated by the growth of amplitudes represented in the bottom panel of Fig. 4(a). Therefore, when $\mathrm{Re} = 0$, the amplitudes a_{2n} and a_{3n} are very small and there is no sign of sidebranching formation.

On the other hand, Fig. 4(b) reveals something different: For this nonzero value of Re, one notices that the morphology of the penetrating inward moving fingers of the outer fluid begins to change, where fingers become slightly sharper at their tips and wider at their sides. By observing the bottom panel of Fig. 4(b), one can see that this suggestive morphological event is due to the favored nonlinear growth of both harmonic modes $2n$ and $3n$, which now have sizable positive amplitudes. Since the only difference between the situations depicted in Figs. 4(a) and 4(b) is the nonzero value of Re used in Fig. 4(b), we can say that the changes in the finger shape shown in Fig. 4(b) are driven by inertial effects.

An even more revealing morphological behavior is observed in Fig. 4(c), where Re is nonzero and larger than the value used in Fig. 4(b). By inspecting the interface depicted in the top panel of Fig. 4(c), one verifies something quite interesting, namely, the evolution of broadened, threefold shaped invading fingers, clearly showing interfacial lobes that branch out sideways. This produces the formation of sidebranching patterns in our Newtonian lifting Hele-Shaw flow system. Such a curious pattern-forming behavior can be justified by resorting to our mode-coupling approach: From the bottom panel of Fig. 4(c) one can see that this scenario is promoted by the enhanced nonlinear growth of mode $3n$ (with the appropriate positive phase), which, jointly with the nonlinear growth of mode $2n$, results in sidebranched finger shapes. All this results from the action of inertia. The onset of sidebranching formation depicted in Fig. 4(c) provides a possible theoretical explanation for the development of complex sidebranching structures (right panel of Fig. 1) detected experimentally in Refs. [20,23,28].

It is worthwhile to point out that the sidebranching phenomenon detected in Fig. 4 is inherently nonlinear and could not be either predicted or captured by a purely linear perturbative description of the lifting Hele-Shaw problem, even if inertial effects are taken into account. To illustrate this important point, in Fig. 5(a) we plot the linear interface shape and in Fig. 5(b) the weakly nonlinear interface shape for $\mathrm{Re} = 0.1$ at time $t_f = 1.3$. The interfaces depicted in Fig. 5 are plotted by using exactly the same physical parameters and initial conditions utilized to produce the patterns depicted in the top panel of Fig. 4. The only difference between Figs. 5(a) and 5(b) is that, while Fig. 5(a) is obtained by numerically solving the purely linear (in ζ) Eq. (16), Fig. 5(b) results from the numerical solution of the second-order $O(\zeta^2)$ mode-coupling equation (7).

By inspecting Fig. 5 it is evident that, despite the consideration of a sizable Reynolds number, one does not observe any tendency towards sidebranching formation in the linear description of the problem [Fig. 5(a)]. Linearly, regardless of the incorporation of inertial effects, the shape of the

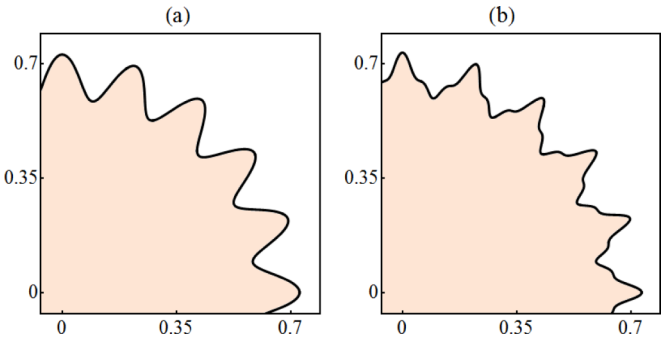

FIG. 5. Snapshot of (a) a linear interface [obtained by solving Eq. (16)] and (b) a weakly nonlinear interface [obtained by solving Eq. (7)], for a Reynolds number Re $= 0.1$, taken at time $t_f = 1.3$. All physical parameters and initial conditions are the same in both (a) and (b) and are identical to those utilized in Fig. 4(c).

pattern is dominated by the growth of fundamental mode n, while the harmonic modes $2n$ and $3n$ just cannot keep up with it. On the other hand, the weakly nonlinear morphology revealed in Fig. 5(b) emerges due to the coupling and enhanced nonlinear growth of modes $2n$ and $3n$. This observation reinforces the necessity of considering the nonlinear interaction among participating modes [through the second-order mode-coupling equations (7)–(15)] in order to get sidebranched morphologies via a perturbative scheme. In spite of the somewhat complicated nature of Eqs. (7)–(15), their use pays off, revealing, already at lowest nonlinear order, the onset of the dentriticlike fingering formation in lifting Hele-Shaw cells with Newtonian fluids.

Before we close our analysis about the occurrence of inertia-induced sidebranching, it should be stressed that we have searched for additional types of patterns within and beyond the range of parameters (Re, Ca, and q) and initial conditions considered in Fig. 4, but have not found any other significantly distinct type of finger morphologies than the representative ones already presented in Fig. 4. By the way, it should be pointed out that we have not been able to identify the development of finger tip splitting in our system. Therefore, at least within the scope of our weakly nonlinear theory, one can say that when Re is sufficiently high, the basic morphological mechanism for Newtonian lifting confined flows is actually finger sidebranching.

Nevertheless, it is still of interest to have an improved understanding of how the sidebranching phenomenon behaves when the capillary number Ca and the initial aspect ratio q are varied. This issue is addressed in Fig. 6, which illustrates how the rescaled perturbation amplitude of the mode $3n$ $[a_{3n}(t)/R(t)]$ varies with time, for three characteristic values of Ca, two values of q, and Re $= 0.1$. To plot Fig. 6 we have used the same set of initial conditions utilized in Fig. 4. As we also did in Fig. 4, the values of n used for each of the situations analyzed in Fig. 6 are set by the condition $\lambda(3n) = 0$, evaluated at $t = t_f = 1.3$.

By examining Fig. 6 it is apparent that, for all these different situations, the rescaled amplitude $a_{3n}(t)/R(t)$ increases with time. This ensures consistent growth of the harmonic mode $3n$ with a positive phase, something that naturally enhances tendency toward finger sidebranching. It is also pretty clear that, larger values of Ca and q lead to augmented sidebranching. These weakly nonlinear findings are consistent with the linear stability results discussed in Sec. III, where we have seen that higher magnitudes of Ca and q do tend to destabilize the system. In any case, from Figs. 4 and 6 we learn that the most favorable conditions for the emergence of dendriticlike structures in our Newtonian lifting flow system are the ones involving larger values of Re, Ca, and q.

B. Influence of inertia on finger competition

Besides the typical format of the fingers discussed in Sec. IV A, as already mentioned in Sec. I, another conspicuous aspect verified during lifting Hele-Shaw flows is the phenomenon of finger

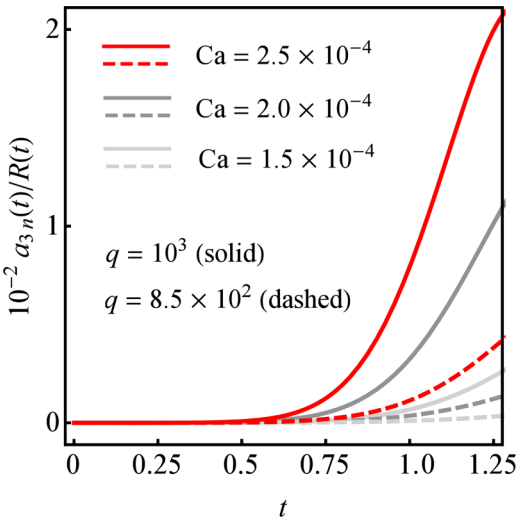

FIG. 6. Rescaled perturbation amplitude $a_{3n}(t)/R(t)$ plotted as a function of time, for Reynolds number $\mathrm{Re} = 0.1$, three values of the capillary number Ca, and two values of the initial aspect ratio q.

competition. Numerical simulations and experiments [17,19,22,23,25,37–39,43] consistently show a competition (i.e., a finger length variability) among the fingers of the invading less viscous fluid, which advance towards the center of the Hele-Shaw cell. Taking into consideration the relevance of the finger competition dynamics to lifting Hele-Shaw flows in general, in this section we examine how it is affected by inertia.

We follow Ref. [12] and consider finger length variability as a measure of the competition among fingers. Within our mode-coupling approach, the finger competition mechanism is described by the influence of a fundamental mode n, assuming n is even, on the growth of its subharmonic mode $n/2$. Similar to what we have done in Sec. IV A, here the equations of motion for the subharmonic mode amplitudes $a_{n/2}$ and $b_{n/2}$ can be obtained by using Eqs. (7)–(15). The mode-coupling finger competition mechanism is based on a very simple idea: The action of the subharmonic mode breaks the n-fold rotational symmetry of the fundamental mode by alternately increasing and decreasing the length of each of the n fingers. This candid mechanism mimics the actual finger competition phenomenon observed in laboratory and numerical experiments of Hele-Shaw flows. It is worth noting that the validity and correctness of this finger competition mechanism for advanced time stages of the Hele-Shaw cell dynamics have already been tested by extensive numerical simulations [57,58].

As discussed in Refs. [12,24], in the scope of the mode-coupling picture, an increased variability among the lengths of fingers of the outer fluid penetrating into the inner fluid corresponds to an increase in the growth of the sine subharmonic mode amplitude $b_{n/2}$ (or, equivalently, to a decrease in the growth of the cosine subharmonic amplitude $a_{n/2}$). This effect describes the competition of inward moving fingers observed in actual lifting Hele-Shaw flows [17,19,22,23,25,37–39,43]. Note that if these behaviors for $a_{n/2}$ and $b_{n/2}$ are reversed, such that modes $a_{n/2}$ would be favored over modes $b_{n/2}$, the mode-coupling description would disclose competition of the outward moving fingers of the inner fluid. However, this is not what is observed in Refs. [17,19,22,23,25,37–39,43].

To exemplify the characteristic impact of inertia on the finger competition behavior, Fig. 7 illustrates a parametric plot of the difference between the sine and the cosine perturbation amplitudes for the subharmonic mode $[b_{n/2}(t) - a_{n/2}(t)]$, relative to the amplitude of the fundamental mode $a_n(t)$. This kind of plot is convenient in the sense that it simultaneously expresses the behavior of both $b_{n/2}(t)$ and $a_{n/2}(t)$ (which are responsible for the finger competition mechanism) with

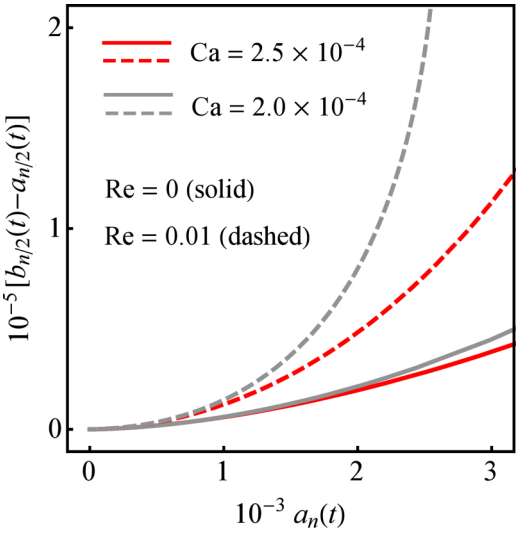

FIG. 7. Parametric plot expressing the behavior of $b_{n/2}(t) - a_{n/2}(t)$ with respect to variations in $a_n(t)$, for two values of the Reynolds number Re and two values of the capillary number Ca.

respect to the growth of the fingers as a whole (provided by the fundamental mode). In Fig. 7 we set two values for the Reynolds number $\mathrm{Re} = 0$ (solid curves) and $\mathrm{Re} = 0.01$ (dashed curves) and two distinct capillary numbers $\mathrm{Ca} = 2.0 \times 10^{-4}$ and 2.5×10^{-4}. In addition, we set $q = 850$. The initial conditions are taken as $a_n(0) = 10^{-7}$, $\dot{a}_n(0) = 5 \times 10^{-7}$, $a_{n/2}(0) = b_{n/2}(0) = 10^{-8}$, and $\dot{a}_{n/2}(0) = \dot{b}_{n/2}(0) = 5 \times 10^{-8}$. Similar to what we did in Fig. 4, the values of n used for each of the situations analyzed are set by the condition $\lambda(n) = 0$ [i.e., the largest Fourier mode between n and $n/2$ is taken as the critical mode], evaluated at $t = t_f = 0.7$. In Fig. 7 one can readily compare the finger competition behavior for the cases with and without inertia.

From Fig. 7, first we verify that the difference $b_{n/2} - a_{n/2}$ increases when the amplitude of the fundamental mode a_n assumes larger values. It turns out that, within the scope of our mode-coupling description, this is precisely the behavior of the subharmonic modes that favors inward finger competition (i.e., prevalence of the growth of $b_{n/2}$ over the growth of $a_{n/2}$). In addition, for any given value of a_n, since the dashed curves are above the corresponding solid ones, it is evident that when $\mathrm{Re} = 0.01$, $b_{n/2} - a_{n/2}$ is larger than for $\mathrm{Re} = 0$. This observation suggests that, due to inertia, nonlinear effects naturally enhance tendency toward competition of the inward fingers. Finally, by inspecting Fig. 7, an interesting aspect of the nonlinear dynamics can be observed: A larger value of Ca leads to a relatively modest inhibition of the inward finger competition, despite the fact that the system is more linearly unstable for higher capillary numbers. This weakly nonlinear theoretical result is consistent with experimental findings of Ref. [25] regarding the role of capillary effects on finger length variability behavior in lifting flows with Newtonian fluids.

V. CONCLUSION

In classical formulations of Hele-Shaw cell problems, the width of the cell gap is constant. In this work we considered the development of viscous fingering patterns in a lifting Hele-Shaw cell with Newtonian fluids, where the cell gap is time dependent. Lifting Hele-Shaw flows at low lifting velocities lead to the emergence of smooth, nonsplitting fingers that compete among themselves. These fingering structures can be appropriately predicted and described by a conventional Darcy law approach, for which inertial effects can be neglected. However, at large lifting speeds, even though the inward moving fingers still compete, completely different dendriticlike patterns are formed.

Seemingly, a theoretical justification for the rising of such peculiar sidebranched patterns still needs to be offered.

In this paper we used a generalized Darcy law description for the Newtonian lifting Hele-Shaw cell problem, which is based on the gap averaging of the 3D Navier-Stokes equation for the system. Within this theoretical scheme, inertial effects are not necessarily negligible and can be properly taken into account. Additionally, we tackled the problem by employing a mode-coupling perturbative approach. Our weakly nonlinear analysis was performed at the lowest (second-order) nonlinear level and was able to capture chief morphological pattern-forming behaviors of the Newtonian confined lifting flow. This was done by considering the coupling of just a few relevant, interacting Fourier modes. In this framework, our theoretical results point to the fact that the rising of the dendriticlike structures detected experimentally in Refs. [20,23,28] is due to inertia. We also found that inertial effects tend to enhance the competition among invading fingers. In conclusion, our work indicates that, depending on the fluid flow circumstances, inertia may have a significant impact on the pattern-formation dynamics of the Newtonian lifting Hele-Shaw cell problem.

A possible extension of this work could address fully nonlinear numerical simulations of the lifting Hele-Shaw problem with Newtonian fluids, now adding the contribution of inertial effects, as prescribed by the nonlinear generalized Darcy law (1). Hopefully, such a numerical study could check some of our weakly nonlinear theoretical findings and also reproduce more accurately the complex advanced time sidebranching structures experimentally revealed in Refs. [20,23,28].

ACKNOWLEDGMENTS

J.A.M. thanks CNPq (Brazilian Research Council) for financial support under Grant No. 304821/2015-2. E.O.D. acknowledges financial support from FACEPE through PPP Project No. APQ-0800-1.05/14.

[1] P. G. Saffman and G. I. Taylor, The penetration of a fluid into a porous medium or Hele-Shaw cell containing a more viscous liquid, Proc. R. Soc. London Ser. A **245**, 312 (1958).

[2] G. M. Homsy, Viscous fingering in porous media, Annu. Rev. Fluid Mech. **19**, 271 (1987); K. V. McCloud and J. V. Maher, Experimental perturbations to Saffman-Taylor flow, Phys. Rep. **260**, 139 (1995); J. Casademunt, Viscous fingering as a paradigm of interfacial pattern formation: Recent results and new challenges, Chaos **14**, 809 (2004).

[3] A. J. DeGregoria and L. W. Schwartz, A boundary-integral method for two-phase displacement in Hele-Shaw cells, J. Fluid Mech. **164**, 383 (1986).

[4] E. Meiburg and G. M. Homsy, Nonlinear unstable viscous fingers in Hele-Shaw flows. II. Numerical simulation, Phys. Fluids **31**, 429 (1988).

[5] C.-W. Park and G. M. Homsy, The instability of long fingers in Hele-Shaw flows, Phys. Fluids **28**, 1583 (1985).

[6] P. Tabeling, G. Zocchi, and A. Libchaber, An experimental study of the Saffman-Taylor instability, J. Fluid Mech. **177**, 67 (1987).

[7] T. Maxworthy, The nonlinear growth of a gravitationally unstable interface in a Hele-Shaw cell, J. Fluid Mech. **177**, 207 (1987).

[8] J. A. Miranda and M. Widom, Weakly nonlinear investigation of the Saffman-Taylor problem in a rectangular Hele-Shaw cell, Int. J. Mod. Phys. B **12**, 931 (1998).

[9] L. Paterson, Radial fingering in a Hele-Shaw cell, J. Fluid Mech. **113**, 513 (1981).

[10] S. N. Rauseo, P. D. Barnes, and J. V. Maher, Development of radial fingering patterns, Phys. Rev. A **35**, 1245 (1987).

[11] S. E. May and J. V. Maher, Fractal dimension of radial fingering patterns, Phys. Rev. A **40**, 1723 (1989).

[12] J. A. Miranda and M. Widom, Radial fingering in a Hele-Shaw cell: A weakly nonlinear analysis, Physica D **120**, 315 (1998).
[13] O. Praud and H. L. Swinney, Fractal dimension and unscreened angles measured for radial viscous fingering, Phys. Rev. E **72**, 011406 (2005).
[14] S. W. Li, J. S. Lowengrub, J. Fontana, and P. Palffy-Muhoray, Control of Viscous Fingering Patterns in a Radial Hele-Shaw Cell, Phys. Rev. Lett. **102**, 174501 (2009).
[15] E. Ben-Jacob, R. Godbey, N. D. Goldenfeld, J. Koplik, H. Levine, T. Mueller, and L. M. Sander, Experimental Demonstration of the Role of Anisotropy in Interfacial Pattern Formation, Phys. Rev. Lett. **55**, 1315 (1985).
[16] H. La Roche, J. F. Fernández, M. Octavio, A. G. Loeser, and C. J. Lobb, Diffusion-limited-aggregation model for Poisson growth, Phys. Rev. A **44**, R6185 (1991).
[17] M. J. Shelley, F.-R. Tian, and K. Wlodarski, Hele-Shaw flow and pattern formation in a time-dependent gap, Nonlinearity **10**, 1471 (1997).
[18] S. Roy and S. Tarafdar, Patterns in the variable Hele-Shaw cell for different viscosity ratios: Similarity to river network geometry, Phys. Rev. E **54**, 6495 (1996).
[19] D. Derks, A. Lindner, C. Creton, and D. Bonn, Cohesive failure of thin layers of soft model adhesives under tension, J. Appl. Phys. **93**, 1557 (2003).
[20] S. Sinha, S. K. Kabiraj, T. Dutta, and S. Tarafdar, Radially interrupted viscous fingers in a lifting Hele-Shaw cell, Eur. Phys. J. B **36**, 297 (2003).
[21] M. Ben Amar and D. Bonn, Fingering instabilities in adhesive failure, Physica D **209**, 1 (2005).
[22] A. Lindner, D. Derks, and M. J. Shelley, Stretch flow of thin layers of Newtonian liquids: Fingering patterns and lifting forces, Phys. Fluids **17**, 072107 (2005).
[23] S. Sinha, T. Dutta, and S. Tarafdar, Adhesion and fingering in the lifting Hele-Shaw cell: Role of the substrate, Eur. Phys. J. E **25**, 267 (2008).
[24] E. O. Dias and J. A. Miranda, Control of radial fingering patterns: A weakly nonlinear approach, Phys. Rev. E **81**, 016312 (2010).
[25] J. Nase, D. Derks, and A. Lindner, Dynamic evolution of fingering patterns in a lifted Hele-Shaw cell, Phys. Fluids **23**, 123101 (2011).
[26] E. O. Dias and J. A. Miranda, Determining the number of fingers in the lifting Hele-Shaw problem, Phys. Rev. E **88**, 043002 (2013).
[27] Z. Zheng, H. Kim, and H. A. Stone, Controlling Viscous Fingering Using Time-Dependent Strategies, Phys. Rev. Lett. **115**, 174501 (2015).
[28] H. Van Damme, in *The Fractal Approach to Heterogeneous Chemistry: Surfaces, Colloids, Polymers*, edited by D. Avnir (Wiley, Chichester, 1989), pp. 199–226.
[29] A. Buka, P. Palffy-Muhoray, and Z. Racz, Viscous fingering in liquid crystals, Phys. Rev. A **36**, 3984 (1987).
[30] H. Zhao and J. V. Maher, Associating-polymer effects in a Hele-Shaw experiment, Phys. Rev. E **47**, 4278 (1993).
[31] L. Kondic, P. Palffy-Muhoray, and M. J. Shelley, Models of non-Newtonian Hele-Shaw flow, Phys. Rev. E **54**, 4536(R) (1996).
[32] L. Kondic, M. J. Shelley, and P. Palffy-Muhoray, Non-Newtonian Hele-Shaw Flow and the Saffman-Taylor Instability, Phys. Rev. Lett. **80**, 1433 (1998).
[33] P. Fast, L. Kondic, M. J. Shelley, and P. Palffy-Muhoray, Pattern formation in non-Newtonian Hele-Shaw flow, Phys. Fluids **13**, 1191 (2001).
[34] M. Constantin, M. Widom, and J. A. Miranda, Mode-coupling approach to non-Newtonian Hele-Shaw flow, Phys. Rev. E **67**, 026313 (2003).
[35] P. Fast and M. J. Shelley, A moving overset grid method for interface dynamics applied to non-Newtonian Hele-Shaw flow, J. Comput. Phys. **195**, 117 (2004).
[36] J. V. Fontana, S. A. Lira, and J. A. Miranda, Radial viscous fingering in yield stress fluids: Onset of pattern formation, Phys. Rev. E **87**, 013016 (2013).
[37] S. K. Kabiraj and S. Tarafdar, Finger velocities in the lifting Hele-Shaw cell, Physica A **328**, 305 (2003).

[38] J. Nase, A. Lindner, and C. Creton, Pattern Formation During Deformation of a Confined Viscoelastic Layer: From a Viscous Liquid to a Soft Elastic Solid, Phys. Rev. Lett. **101**, 074503 (2008).
[39] S. Tarafdar, S. Nag, T. Dutta, and S. Sinha, Computer simulation of viscous fingering in a lifting Hele-Shaw cell with grooved plates, Pramana **73**, 743 (2009).
[40] P. Gondret and M. Rabaud, Shear instability of two-fluid parallel flow in a Hele-Shaw cell, Phys. Fluids **9**, 3267 (1997).
[41] C. Ruyer-Quil, Inertial corrections to the Darcy law in a Hele-Shaw cell, C. R. Acad. Sci. Ser. II B **329**, 337 (2001).
[42] F. Plouraboue and E. J. Hinch, Kelvin-Helmholtz instability in a Hele-Shaw cell, Phys. Fluids **14**, 922 (2002).
[43] C. Chevalier, M. Ben Amar, D. Bonn, and A. Lindner, Inertial effects on Saffman-Taylor viscous fingering, J. Fluid Mech. **552**, 83 (2006).
[44] A. He and A. Belmonte, Inertial effects on viscous fingering in the complex plane, J. Fluid Mech. **668**, 436 (2011).
[45] E. O. Dias and J. A. Miranda, Inertial effects on rotating Hele-Shaw flows, Phys. Rev. E **83**, 046311 (2011).
[46] E. O. Dias and J. A. Miranda, Influence of inertia on viscous fingering patterns: Rectangular and radial flows, Phys. Rev. E **83**, 066312 (2011).
[47] Q. Yuan and J. Azaiez, Inertial effects of miscible viscous fingering in a Hele-Shaw cell, Fluid Dyn. Res. **47**, 015506 (2015).
[48] Q. Yuan and J. Azaiez, Inertial effects in cyclic time-dependent displacement flows in homogeneous porous media, Can. J. Chem. Eng. **93**, 1490 (2015).
[49] H. Guo, D. C. Hong, and D. A. Kurtze, Surface-Tension-Driven Nonlinear Instability in Viscous Fingers, Phys. Rev. Lett. **69**, 1520 (1992).
[50] H. Guo, D. C. Hong, and D. A. Kurtze, Dynamics of viscous fingers and threshold instability, Phys. Rev. E **51**, 4469 (1995).
[51] E. Alvarez-Lacalle, J. Casademunt, and J. Ortín, Systematic weakly nonlinear analysis of interfacial instabilities in Hele-Shaw flows, Phys. Rev. E **64**, 016302 (2001).
[52] E. Alvarez-Lacalle, E. Pauné, J. Casademunt, and J. Ortín, Systematic weakly nonlinear analysis of radial viscous fingering, Phys. Rev. E **68**, 026308 (2003).
[53] L. N. Brush, R. F. Sekerka, and G. B. McFadden, A numerical and analytical study of nonlinear bifurcations associated with the morphological stability of two-dimensional single crystals, J. Cryst. Growth **100**, 89 (1990).
[54] P. P. Debroy and R. F. Sekerka, Weakly nonlinear morphological instability of a cylindrical crystal growing from a pure undercooled melt, Phys. Rev. E **53**, 6244 (1996).
[55] E. Alvarez-Lacalle, J. Ortín, and J. Casademunt, Low viscosity contrast fingering in a rotating Hele-Shaw cell, Phys. Fluids **16**, 908 (2004).
[56] H. Gadêlha and J. A. Miranda, Finger competition dynamics in rotating Hele-Shaw cells, Phys. Rev. E **70**, 066308 (2004).
[57] J. A. Miranda and E. Alvarez-Lacalle, Viscosity contrast effects on fingering formation in rotating Hele-Shaw flows, Phys. Rev. E **72**, 026306 (2005).
[58] C.-Y. Chen, C.-H. Chen, and J. A. Miranda, Numerical study of pattern formation in miscible rotating Hele-Shaw flows, Phys. Rev. E **73**, 046306 (2006).
[59] R. Folch, E. Alvarez-Lacalle, J. Ortín, and J. Casademunt, Pattern formation and interface pinch-off in rotating Hele-Shaw flows: A phase-field approach, Phys. Rev. E **80**, 056305 (2009).
[60] R. Brandão, J. V. Fontana, and J. A. Miranda, Suppression of viscous fingering in nonflat Hele-Shaw cells, Phys. Rev. E **90**, 053003 (2014).
[61] P. H. A. Anjos and J. A. Miranda, Influence of wetting on fingering patterns in lifting Hele-Shaw flows, Soft Matter **10**, 7459 (2014).
[62] J. V. Fontana, H. Gadêlha, and J. A. Miranda, Development of tip-splitting and side-branching patterns in elastic fingering, Phys. Rev. E **93**, 033126 (2016).
[63] M. Zhao, A. Belmonte, S. Li, X. Li, and J. S. Lowengrub, Nonlinear simulations of elastic fingering in a Hele-Shaw cell, J. Comput. Appl. Math. **307**, 394 (2016).